Meteoritics & Planetary Science 38, Nr 8, 1199–1215 (2003)
Abstract available online at http://meteoritics.org

Evidence for fractional condensation and reprocessing at high temperatures in CH chondrites

Dominik C. HEZEL,[1*] Herbert PALME,[1] Frank E. BRENKER,[1] and Lutz NASDALA[2]

[1]Universität zu Köln, Institut für Mineralogie und Geochemie, Zülpicherstr. 49b, D-50674 Köln, Germany
[2]Johannes-Gutenberg Universität Mainz, Institut für Geowissenschaften-Mineralogie, Becherweg 21, D-55099 Mainz, Germany
[*]Corresponding author. E-mail: d.hezel@uni-koeln.de

(Received 18 December 2002; revision accepted 10 June 2003)

Abstract–We performed a detailed study of silica-rich components (SRC) in the paired CH chondrites Acfer 182 and 207. These SRCs appear either as chondrules or fragments, and they contribute <0.1 vol% to the bulk meteorite. They usually contain a silica and a silicate portion. Both portions are, in most cases, cryptocrystalline and have bulk SiO_2-concentrations between 65 and 85 wt%. The silicate generally has a pyroxene normative composition. The silica often appears as blebs within the silicate matrix or vice versa. If there are no blebs, silica and silicate still form rounded interfaces. The SRCs are depleted in refractory elements like Ca, Al, and Ti relative to CI. A few SRC- like objects are extremely rich in Mn and show no depletion in refractory elements. We conducted micro-Raman studies on the silica portions of the SRCs to determine their structure, and we identified several silica phases: α-quartz, cristobalite, glass, and a yet unidentified polymorph. The silicate portion is glass when the silica is glass and crystalline when the silica is crystalline.

The low contents of Al and Ca make an igneous origin of the SRCs very unlikely, and the absence of metal excludes the formation by reduction of pyroxene. We suggest, instead, a fractional condensation origin of the SRCs from a Si-enriched gas after removal of gaseous Mg by forsterite condensation. Additional evidence for fractional condensation is provided by a unique layered object with olivine in the core, pyroxene and metal at the rim, and silica at the outermost border; these layers record the condensation sequence. Two chondrules were found with several percent of Mn and high Cr, Na, and K contents, providing further evidence for condensation from a fractionated gas.

The texture of the SRCs and the occurrence of cristobalite and silica glass, however, require formation by liquid immiscibility at high temperatures, above 1968 K, and subsequent fast cooling. Therefore, we propose a 2-stage model for the formation of SRCs in CH chondrites: 1) fractional condensation of forsterite, enstatite, and SiO_2-rich phases; and 2) reheating of SiO_2-rich components to temperatures above 1968 K followed by rapid cooling.

All other phases identified in CH chondrites can be understood within the framework of this model. Thus, the extremely unequilibrated CH chondrites provide a wealth of evidence for fractional condensation processes in the early solar nebula, in metals (Meibom et al. 1999), and in silicates.

INTRODUCTION

The CH chondrites are a recently recognized meteorite group that was introduced by Bischoff et al. (1993). Seven members of this group are known to date: Acfer 182, Allan Hills (ALH) 85085, Elephant Moraine (EET) 96238, Northwest Africa (NWA) 470, Patuxent Range (PAT) 91546, Pecora Escarpment (PCA) 91467, and Reckling Peak (RKP) 92435 (Koblitz 2000; Ivanova et al. 2001). Members of the unequilibrated CH chondrites are among the most primitive meteorites within the carbonaceous chondrite suite. Their pristine nature provides direct information about processes in the early solar nebula.

The CH chondrites are characterized by: 1) unfractionated refractory lithophile element abundances and strong depletions in moderately volatile and highly volatile elements (Mn, Na, Zn, Se) but with an excess of Fe and other nonvolatile siderophile elements; 2) 70 vol% of 20–90 μm small chondrules and chondrule fragments. The latter are derived from a group of initially larger chondrules, possibly up to several hundred microns in diameter (e.g., Scott 1988; Weisberg et al. 1988; Bischoff et al. 1993); 3) 20 vol% FeNi-

metal grains with significant amounts of Cr. Metal grains are occasionally zoned with respect to Ni, Co, and refractory metals, which is indicative of condensation (Meibom et al. 1999, 2000; Campbell and Humayun 2002); 4) low FeO-contents in silicates and high Cr in metal, reflecting reducing conditions (Scott 1988); 5) a low abundance of CAIs, around 0.1 vol%; 6) no secondary alteration of CAIs, chondrules, and chondrule fragments; 7) a lack of matrix, except for Acfer 182, which has about 5 vol% of a volatile-rich and hydrated matrix that was heavily altered by terrestrial weathering and is mostly present as matrix lumps (Krot et al. 2002 and references therein); 8) a population of silica-rich components (SRC), described by Petaev and Krot (1999), Petaev et al. (2001), and Hezel et al. (2002a, b); and 9) a population of "ferrous silicate spherules with euhedral iron-nickel metal grains" (Krot et al. 2000a).

The chemical composition and the petrography of the first CH meteorite, ALH 85085, of Antarctic origin were discussed in a series of papers by Scott (1988), Weisberg et al. (1988), and Grossman et al. (1988). The chemistry and petrography of CH desert meteorites are given by Bischoff et al. (1993) and Weisberg et al. (1995). A recently published review by Krot et al. (2002) summarizes the present knowledge of the CR chondrite clan, including CH chondrites. According to Bischoff et al. (1993) and Weisberg et al. (1995), CH chondrites are closely related to the CR and CB chondrites in having a large excess of metal and similar chemical compositions of silicates. (CB chondrites are also known as "Bencubbin-like" chondrites. The term was introduced by Weisberg et al. [2001] but is not well- established. However, the term is mentioned in several recent papers and abstracts, e.g., Greshake et al. [2002]; Krot et al. [2002].) Therefore, Weisberg et al. (1995) have suggested combining these 3 groups into the so called "CR-clan." All members of this clan belong to the petrologic types 2 and 3 and are among the chemically and mineralogical least altered chondrites known to date.

The CH and CB chondrites are more closely related to each other than to the CR chondrites. Both CH and CB chondrites have high modal abundances of FeNi-metal and are enriched in siderophile and strongly depleted in volatile elements. The CR chondrites contain mainly Mg-rich porphyritic chondrules, a few percent of metal, either in matrix or in chondrules, and approximately 40–60 vol% matrix. Petrographically, the CH chondrites appear intermediately between CR and CB chondrites, i.e., they comprise the 2 different chondrule populations of these 2 chondrite types: 1) porphyritic (including radial) chondrules, as in the CR chondrites, and 2) cryptocrystalline (CC), barred olivine (BO), and skeletal olivine (SO) chondrules, as in CB chondrites. The CH chondrites are recognized as regolith breccias according to their noble gas content and because most of their components are fragments (Bischoff et al. 1993).

Several models were proposed for the formation of CH chondrites and their individual components. Wasson (1988) and Wasson and Kallemeyn (1990) proposed the formation of cryptocrystalline chondrules and metals in CH chondrites in a cloud of impact ejecta after the collision of 2 asteroids. However, others (e.g., Grossman et al. 1988; Scott 1988; Weisberg et al. 1988; Bischoff et al. 1993) argued that CH chondrules formed in a similar fashion as chondrules from other chondrite groups. Meibom et al. (1999) explained zoning patterns in individual metal grains of CH chondrites by fractional condensation during cooling from an evaporated nebular region. Recently, Krot et al. (2001) suggested that the CC and SO chondrules in CH and CB chondrites condensed from an evaporated nebular region before metal formation and were then removed from the nebula before volatile element condensation.

The SRCs occur in all types of chondrites but are rare objects, especially in carbonaceous chondrites (e.g., Brigham et al. 1986). They are not predicted by equilibrium condensation (e.g., Ebel and Grossman 2000). Therefore, SRCs require special conditions for their formation by condensation, e.g., a fractionated gas. We performed detailed petrographic and petrologic studies of SRCs in the paired CH chondrites Acfer 182 (1 thin section) and Acfer 207 (2 thin sections; Table 1), which are hereafter designated as Acfer 182. The results of this study provide a model for the formation of CH chondrites, including some aspects of the proposed models described above.

ANALYTICAL TECHNIQUES

Mineral analyses were made with the electron microprobe (EMP) JEOL 8900RL of the Institute of Mineralogy and Geochemistry at the University of Cologne. The accelerating voltage was set to 15 kV and the beam current to 20 nA. The ZAF-algorithm was used for correction. Cathodoluminescence images were taken with a black and white detector mounted on the EMP. Most back scattered electron (BSE) images were taken with the EMP. For some of the BSE-images, we used the JEOL JSM5900 scanning electron microprobe at the University of Hawai'i at Manoa.

Silica-rich components can be identified either with Si-element maps or with a CL detector, under which they appear bright. CL imaging has the advantage of being much faster. Figure 1 shows 2 examples of SRCs in a CL image (corresponding to Figs. 2a and 2b).

Table. 1. Statistic of analyzed silica-rich components (SRCs) in CH chondrites.[a]

Meteorite	SRCs	glass	crs	u.p.	crs & qtz	qtz
Acfer 182	12	4	2	1	1	1
Acfer 207-I	8	–	1	–	1	2
Acfer 207-II	4	–	–	–	–	–

[a]The numbers in the column "SRCs" give the amount of analyzed SRCs. The other columns show how many SRCs contain a specific polymorph. The sum from the different silica polymorphs do not match the amount of total SRCs because we did not analyze all silica in the SRCs for their polymorph. "u.p." is an unknown polymorph (see text).

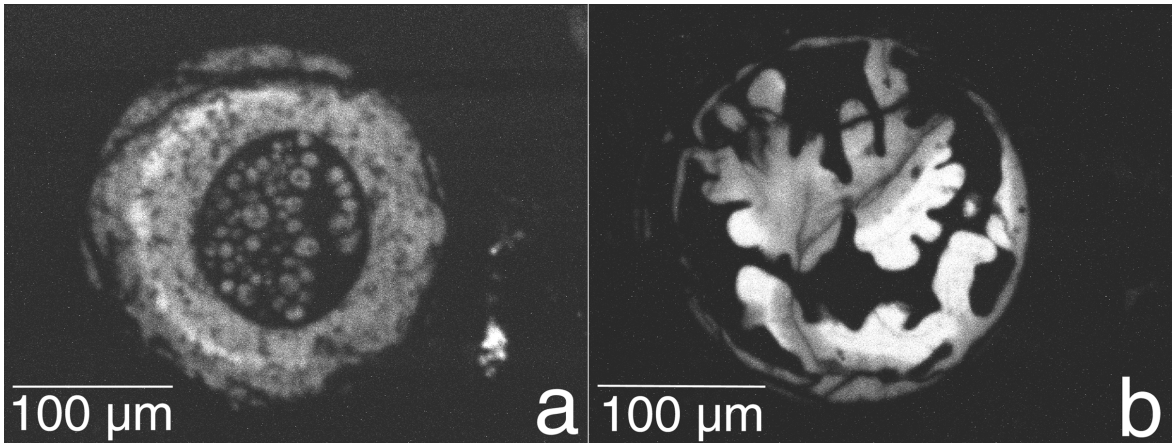

Fig. 1. Two silica-rich components. The pictures were taken with the CL detector. The silica is bright, while the silicate is dark. The pictures correspond to the 2 BSE images of Figs. 2a and 2b.

Thirteen SRCs were studied with Raman microprobe analysis. The measurements were done by means of a Jobin Yvon (Horiba) LabRam HR800 system. This notch filter-based spectrometer was equipped with an Olympus BX41 microscope, a grating with 1800 grooves per mm, and a Si-based charge-coupled device (CCD) detector. The spectra were excited with the He-Ne 632.8 nm emission (3 mW). With the Olympus 100× objective, the lateral resolution was better than 1.5 µm. The wave number accuracy was 0.5 cm^{-1}, and the spectral resolution was 0.5 cm^{-1}.

One SRC in Acfer 182 and 1 unknown SiO_2 polymorph were subjected to transmission-electron microscopy (TEM) analysis. The TEM studies were performed with a Phillips CM30 at the University of Bonn with an accelerating voltage of 300 kV. For TEM analysis of Acfer 182, a piece 3 mm in diameter was removed from the thin section and mounted on a copper grid. The sample was then ion-thinned until it reached electron transparency. By monitoring the thinning process with regular BSE analysis, we were able to achieve thinning exactly at the locations required for the study of the SiO_2 phases. Small pieces from the unknown SiO_2 polymorph were cut from the thin section and crushed between 2 glass slides to produce small fragments transparent to high energy electrons and, therefore, suitable for TEM work.

All of the mineral abbreviations used follow the suggestions of Kretz (1983). The mineral abbreviations not listed by Kretz (1983) are explained in the text.

RESULTS

The main components of the CH chondrites are porphyritic (~70 vol%) and cryptocrystalline chondrules and chondrule fragments and FeNi-metals (20 vol%). Matrix occurs with ~5 vol% (only in Acfer 182; the other CHs lack matrix) and CAIs with about 0.1 vol% (e.g., Scott 1988; Weisberg et al. 1988; Bischoff et al. 1993; Meibom et al. 1999). In addition, we identified 2 components that were not discussed in detail before. These are: 1) silica-rich components (SRC) and 2) large fragments of feldspar grains >200 µm in length. The SRCs are the main focus of this paper, as they provide evidence for fractional condensation in the solar nebula.

Definition and General Petrography of SRCs

The occurrence of silica-rich components in CH chondrites has been mentioned briefly in several abstracts, e.g., Petaev and Krot (1999), Petaev et al. (2001), and Hezel et al. (2002a, b), as well as in a paper by Krot et al. (2000a), but they were never studied in detail. In this paper, we investigated 25 SRCs in Acfer 182. We define SRCs as components with bulk SiO_2-concentrations >65 wt% that usually contain abundant pure SiO_2-phases and silica grains, respectively. Silica in Ca-, Al-rich mesostasis of chondrules is not considered here because this silica crystallized from silica-enriched residual chondrule melts and, therefore, has a different origin than SRCs.

Silica-rich objects constitute a small but common population in ordinary chondrites (e.g., Brigham et al. 1986), but they are nearly absent in carbonaceous chondrites. Although CH chondrites contain comparatively high fractions of SRCs, their modal abundance is still below 0.1 vol%. Most SRC chondrules and fragments range in size from about 100 to over 200 µm. This is significantly larger than the mean chondrule diameter in Acfer 182, which is below 90 µm (Scott 1988). The SRC-paragenesis is virtually metal- and sulfide-free and consists of a silica and a silicate phase, which mostly appear cryptocrystalline.

Appearance of Typical SRCs (Figs. 2a–2f, 2i–2k, and 2m–2o)

Figure 2 emphasizes the variety of SRC appearances. As can be seen, their shapes are quite variable: some of them are

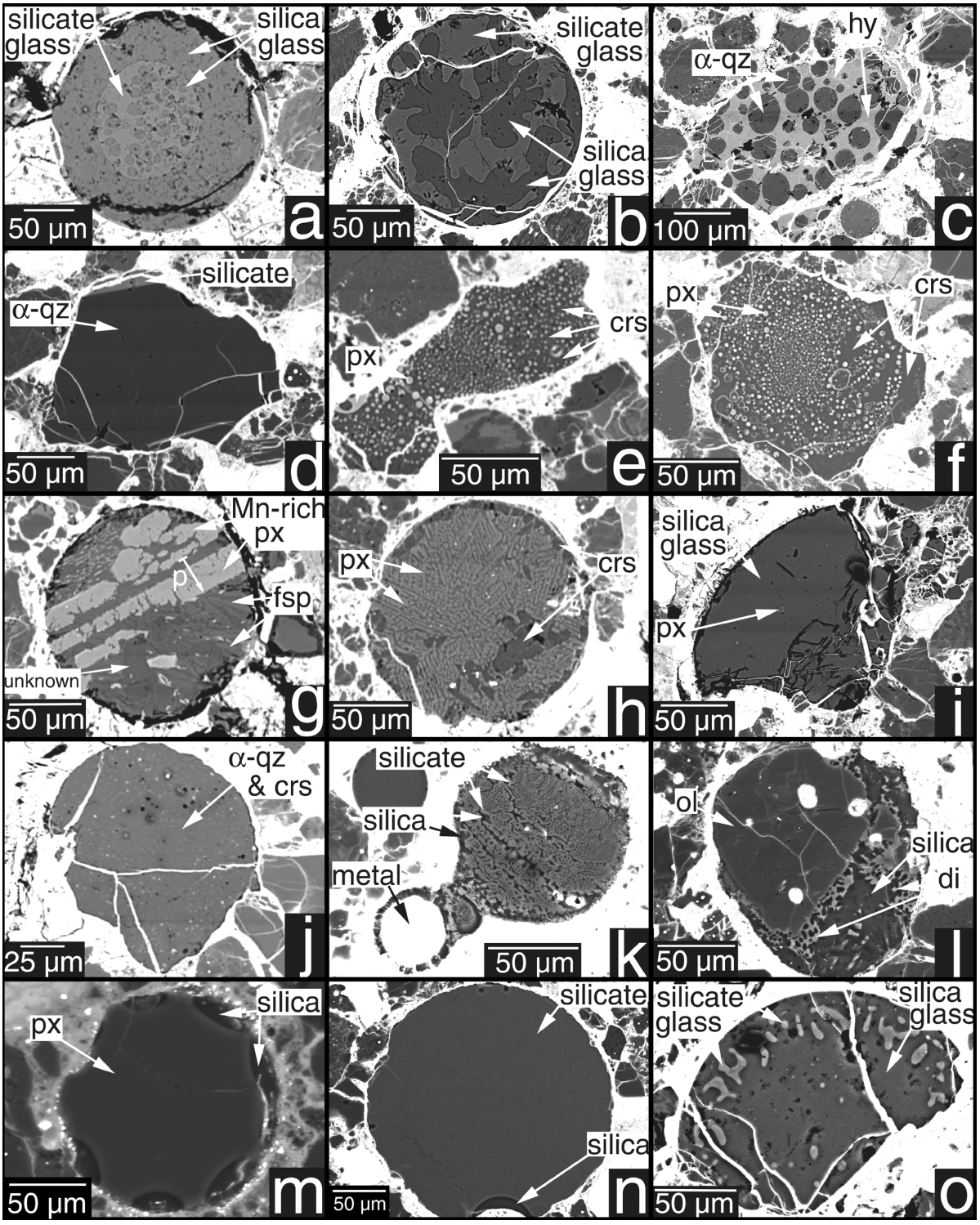

Fig. 2. BSE-images demonstrating variable appearances of SRCs. The most common type contains silica blebs within a silicate matrix or vice versa. The profile marked "p" in image 2g is shown in Fig. 5. See the text for detailed descriptions.

round objects, resembling chondrules (e.g., Fig. 2a), many are angular fragments (e.g., Fig. 2f), and some are obviously chondrule fragments (e.g., Fig. 2i). Furthermore, the textures of SRCs show some variety. In most SRCs, silica occurs either as spherules in a silicate matrix or vice versa as silicate spherules in a silica matrix (Figs. 2a, 2c, 2e, 2f, 2i, 2m, and 2n). The fragment shown in Fig. 2e contains both numerous spherules in a silica matrix and, at the lower left, silica spherules in a bleb of silicate. In some SRCs, silica is exclusively located at the edge of chondrules (Figs. 2m and

2n). One extraordinary object is divided into a silicate core containing silica spherules and a surrounding silica mantle (Figs. 1a and 2a).

Variations of this texture with spherules of 1 phase enclosed in the other are: 1) amoeboid or cockscomb shaped textures of silica occurring within silicate matrix (Figs. 1b and 2b); 2) tightly folded silicate within a silica matrix, as in the unique object shown in Fig. 2k; and 3) small fractions of silicate enclosed in silica, as in Fig. 2o. The silicate is concentrated in a ring near the rim of the object and shows a symplectitic structure.

A different appearance is shown in Fig. 2d. Here, a comparatively large and very coarse-grained silica fragment occurs in the matrix. The silica grain is 220 μm in diameter and has little mesostasis attached to its top. The host chondrule of this fragment must have been much larger. Other SRCs consist of nearly pure silica. These are often very small objects, a few tenths of microns in diameter, but they can also be large, like the 2 pure silica SRCs shown in Figs. 2i and 2j. Sometimes these SRCs contain very tiny droplets of silicates, as in Fig. 2i. The last SRC variation to be mentioned has an ostentatiously smaller diameter than all other SRCs, which, in most cases, does not exceed 20 μm. Members of this group typically occur as cryptocrystalline silicate chondrules with silica spherules at their rims and often contain rounded to euhedral FeNi-metal grains (Krot et al. 2000a). Not all of these objects contain silica spherules and, therefore, not all of them can be called SRCs.

Appearance of Non-Typical SRC Objects (Figs. 2g, 2h, and 2l; Fig. 3)

Some SiO_2-rich objects differ in texture from the SRCs described above but are similar in having high SiO_2-concentrations or free SiO_2. These objects consist of more than 2 phases and no spherules of silica exist in silicate or vice versa. Instead, these objects contain large crystals of pyroxenes or olivines and, in addition, occasionally feldspars (Figs. 2g, 2h, and 2l). Although we do not consider these objects as members of the typical SRC-group, apparently, a relationship exists between the typical SRCs and these objects, as will be discussed in a later section.

A unique and striking object that resembles SRCs is shown in Fig. 3. This is a type IAB chondrule (e.g., Brearley and Jones 1998, and references therein), as it contains coarse-grained olivine and pyroxene crystals and Ca-, Al-rich crystalline mesostasis enclosing the olivines. The remarkable feature of this chondrule is its unusual layering: olivine in the core, metals and pyroxenes at the rim, and silica at the outermost border.

In the 2 objects of Figs. 2g and 2h, silica occurs as randomly distributed mineral grains. In contrast to typical SRCs, they contain well-defined pyroxene crystals. The first object (Fig. 2g) has several large pyroxene crystals of up to 150 μm in length and several tiny pyroxene crystals a few

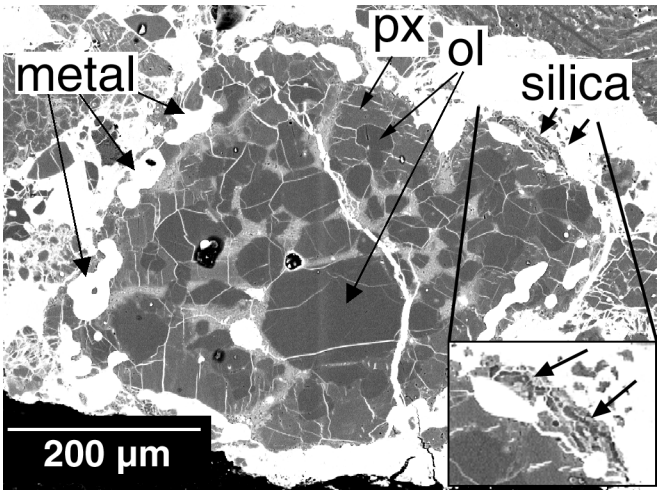

Fig. 3. BSE image of a layered object with olivine in the core, surrounded by pyroxene and metal, and with SiO_2 at the outermost rim. This sequence is predicted by models of fractional condensation.

microns in length, mainly concentrated at the top left. The second object (Fig. 2h) consists of homogeneously distributed, μm-sized pyroxene laths intergrown with tiny feldspars. Silica crystals between 10 and 40 μm in diameter are heterogeneously distributed within and along the rim of the chondrule.

Further, some objects were found that are related to SRCs. They contain large olivine crystals (Fig. 2l) but are not SRCs according to the definition given above because they have less than 65 wt% SiO_2. However, these objects contain silica as laths and blebs in a glassy silicate mesostasis. The large olivines are surrounded by a 10 to 15 μm thin irregular layer of diopside, which contains abundant silica blebs. However, these objects do not resemble typical type I chondrules in Acfer 182, where the mesostasis is a more or less fine-grained intergrowth of silica, feldspar, and occasionally pyroxenes, and the olivines are not usually rimmed by a layer of diopside.

Chemical Composition of SRCs

The silicate phase of typical SRCs is usually relatively Mg-rich with FeO <3–4 wt%, but higher FeO-concentrations of up to 27.39 wt% are not uncommon (Table 2). The silicate is, in most cases, nearly pyroxene normative with a sometimes slightly SiO_2-oversaturated composition. However, this oversaturation can be an artifact when silicate and SiO_2 are tightly intergrown. Then, beam overlap can increase artificially the amount of SiO_2 in the silicate analysis. The silica portion is usually nearly pure SiO_2. However, some silica analysis can also be altered due to beam overlap, and then, the silica analysis can decrease significantly below 100 wt%. For example, the tiny silicate spherules in Figs. 2e and 2f are too small to be analyzed correctly with EMP.

Bulk chemical compositions of SRCs are quite variable

Table 2. Chemical compositions of the silicate and silica portions in different SRCs and bulk compositions of these SRCs.[a]

	Fig. 2a				Fig. 2b			Fig. 2c			Fig. 2d
	Mes Core	SiO_2 Core	SiO_2 Rim	Bulk	Mes	SiO_2	Bulk	Hy	α-Qtz	Bulk	α-Qtz
SiO_2	59.22	96.87	97.09	85.20	59.48	99.30	84.48	52.39	98.53	69.46	97.01
TiO_2	0.19	0.02	0.01	0.07	0.18	0.03	0.09	0.01	0.01	0.01	0.04
Al_2O_3	5.00	0.61	0.29	1.77	5.26	0.32	2.16	0.48	0.17	0.36	0.02
Cr_2O_3	0.29	0.01	0.01	0.10	0.32	0.00	0.12	0.43	0.01	0.28	0.01
FeO	1.40	0.30	0.34	0.67	0.93	0.14	0.43	27.09	1.48	17.61	0.54
MnO	0.02	0.02	0.00	0.01	0.00	0.02	0.01	0.06	0.01	0.04	0.00
NiO	0.03	0.02	0.01	0.02	0.00	0.00	0.00	0.32	0.03	0.22	0.00
MgO	30.24	0.58	0.35	9.74	30.78	0.35	11.66	18.67	0.30	11.87	0.02
CaO	4.17	0.12	0.09	1.37	3.71	0.11	1.45	0.18	0.05	0.13	0.01
Na_2O	0.15	0.07	0.04	0.08	0.01	0.02	0.02	0.10	0.11	0.11	0.00
K_2O	–	–	–	–	–	–	–	–	–	–	–
Total	100.71	98.61	98.25	99.02	100.66	100.28	100.42	99.73	100.70	100.09	97.65
Si	1.987	0.987	0.992	–	1.988	0.993	–	1.999	0.989	–	0.997
Ti	0.005	0.000	0.000	–	0.005	0.000	–	0.000	0.000	–	0.000
Al	0.198	0.007	0.004	–	0.207	0.004	–	0.022	0.002	–	0.000
Cr	0.008	0.000	0.000	–	0.008	0.000	–	0.013	0.000	–	0.000
Fe	0.039	0.003	0.003	–	0.026	0.001	–	0.864	0.012	–	0.005
Mn	0.001	0.000	0.000	–	0.000	0.000	–	0.002	0.000	–	0.000
Ni	0.001	0.000	0.000	–	0.000	0.000	–	0.010	0.000	–	0.000
Mg	1.513	0.009	0.005	–	1.533	0.005	–	1.062	0.004	–	0.000
Ca	0.150	0.001	0.001	–	0.133	0.001	–	0.007	0.001	–	0.000
Na	0.010	0.001	0.001	–	0.000	0.000	–	0.007	0.002	–	0.000
K	–	–	–	–	–	–	–	–	–	–	–
Total	3.910	1.009	1.006	–	3.900	1.005	–	3.987	1.011	–	1.003

	Fig. 2e			Fig. 2f			Fig. 2g			
	Hy	Crs	Bulk	Hy	Crs	Bulk	Mn-rich Px	"Pl"	Unknown	Bulk
SiO_2	52.36	90.91	73.95	56.81	95.79	79.81	51.87	69.04	99.20	72.34
TiO_2	0.03	0.00	0.01	0.00	0.02	0.01	0.41	0.32	0.03	0.26
Al_2O_3	0.15	0.17	0.16	0.19	0.07	0.11	2.77	18.13	0.24	6.05
Cr_2O_3	0.47	0.08	0.25	1.23	0.04	0.52	1.46	0.03	0.01	0.59
FeO	27.39	5.25	14.99	24.29	1.38	10.77	8.38	1.16	0.32	3.74
MnO	0.18	0.05	0.11	0.11	0.01	0.06	6.27	0.35	0.05	2.59
NiO	0.22	0.04	0.12	0.33	0.03	0.15	0.01	0.04	0.03	0.02
MgO	16.95	2.63	8.93	15.44	0.27	6.49	16.09	0.47	0.02	6.51
CaO	0.18	0.02	0.09	0.15	0.02	0.07	13.07	4.63	0.04	6.43
Na_2O	0.28	0.47	0.38	0.03	0.05	0.04	0.16	5.42	0.09	1.55
K_2O	0.04	–	–	0.00	0.02	0.04	0.03	0.47	0.02	0.14
Total	98.25	99.63	99.00	98.58	97.69	98.09	100.54	100.05	100.03	100.24
Si	2.033	0.952	–	2.140	0.990	–	1.927	3.021	0.995	–
Ti	0.001	0.000	–	0.000	0.000	–	0.012	0.011	0.000	–
Al	0.007	0.002	–	0.008	0.001	–	0.121	0.935	0.003	–
Cr	0.015	0.001	–	0.037	0.000	–	0.043	0.001	0.000	–
Fe	0.889	0.046	–	0.765	0.012	–	0.261	0.042	0.003	–
Mn	0.006	0.000	–	0.004	0.000	–	0.197	0.013	0.000	–
Ni	0.007	0.000	–	0.010	0.000	–	0.000	0.001	0.000	–
Mg	0.981	0.041	–	0.867	0.004	–	0.892	0.031	0.000	–
Ca	0.008	0.000	–	0.006	0.000	–	0.520	0.217	0.000	–
Na	0.021	0.009	–	0.002	0.001	–	0.012	0.460	0.002	–
K	–	–	–	–	–	–	–	–	–	–
Total	3.966	1.052	–	3.839	1.009	–	3.985	4.731	1.004	–

Table 2. Chemical compositions of the silicate and silica portions in different SRCs and bulk compositions of these SRCs.[a] *Continued.*

	Fig. 2h				Fig. 2i		Fig. 2j	Fig. 2k		
	Mn-rich Px	"Pl"	Crs	Bulk	Glassy Mes	SiO_2	Qtz & Crs	Px	Silica n.r.	Bulk
SiO_2	56.54	62.11	98.68	65.48	59.01	95.98	97.14	57.84	95.52	71.97
TiO_2	0.34	0.29	0.06	0.28	0.11	0.01	0.00	0.04	0.03	0.04
Al_2O_3	5.70	17.47	0.33	7.79	4.10	0.46	0.08	0.67	1.39	0.94
Cr_2O_3	2.27	0.66	0.03	1.46	0.72	0.01	0.01	0.94	0.07	0.61
FeO	2.56	0.88	0.86	1.82	0.91	0.28	0.40	3.65	0.85	2.60
MnO	3.09	0.93	0.04	1.99	0.01	0.01	0.01	0.52	0.11	0.37
NiO	0.03	0.02	0.05	0.03	0.03	0.01	0.04	0.04	0.07	0.05
MgO	22.34	6.50	0.05	14.27	30.41	0.60	0.19	35.82	2.33	23.26
CaO	7.47	9.21	0.10	6.61	3.54	0.11	0.35	0.92	0.17	0.64
Na_2O	0.67	2.63	0.13	1.08	0.15	0.40	0.03	0.09	0.67	0.31
K_2O	0.03	0.10	0.00	–	0.06	–	–	–	–	–
Total	101.04	100.81	100.31	100.81	99.06	97.86	–	100.54	101.20	100.78
Si	1.960	2.761	0.991	–	2.008	0.987	0.994	1.971	0.961	–
Ti	0.009	0.010	0.000	–	0.003	0.000	0.000	0.001	0.000	–
Al	0.233	0.915	0.004	–	0.164	0.006	0.001	0.027	0.017	–
Cr	0.062	0.023	0.000	–	0.019	0.000	0.000	0.025	0.001	–
Fe	0.074	0.033	0.007	–	0.026	0.002	0.003	0.104	0.007	–
Mn	0.091	0.035	0.000	–	0.000	0.000	0.000	0.015	0.001	–
Ni	0.001	0.001	0.000	–	0.001	0.000	0.000	0.001	0.001	–
Mg	1.154	0.431	0.001	–	1.542	0.009	0.003	1.820	0.035	–
Ca	0.277	0.439	0.001	–	0.129	0.001	0.004	0.034	0.002	–
Na	0.045	0.227	0.002	–	0.010	0.008	0.001	0.006	0.013	–
K	–	–	–	–	–	–	–	–	–	–
Total	3.906	4.874	1.008	–	3.903	1.014	1.006	4.005	1.037	–

	Fig. 2m	Fig. 2n	Fig. 2o		
	Px	Silica oversat.	Glassy Mes	SiO_2	Bulk
SiO_2	55.34	61.79	58.84	95.72	68.25
TiO_2	0.09	0.15	0.23	0.06	0.08
Al_2O_3	0.04	3.54	7.53	0.80	3.19
Cr_2O_3	0.76	1.11	0.14	0.02	0.54
FeO	7.79	2.26	0.61	0.66	0.75
MnO	0.09	1.24	0.01	0.03	0.01
NiO	0.05	0.04	0.01	0.04	0.03
MgO	34.42	25.43	24.92	0.94	22.96
CaO	0.15	2.81	7.37	0.36	2.69
Na_2O	0.00	0.43	0.11	0.08	0.22
K_2O	0.01	–	–	–	–
Total	98.74	98.82	99.78	98.70	98.76
Si	1.954	2.110	1.992	0.980	–
Ti	0.002	0.004	0.006	0.000	–
Al	0.002	0.143	0.301	0.010	–
Cr	0.021	0.030	0.004	0.000	–
Fe	0.230	0.065	0.017	0.006	–
Mn	0.003	0.036	0.000	0.000	–
Ni	0.001	0.001	0.000	0.000	–
Mg	1.812	1.295	1.258	0.014	–
Ca	0.006	0.103	0.267	0.004	–
Na	0.000	0.029	0.007	0.002	–
K	0.000	–	–	–	–
Total	4.032	3.814	3.853	1.016	–

[a]Some mesostases are calculated with 6 oxygens and resemble pyroxene compositions. The plagioclase analyses in Figs. 2g and 2h are not very good. This may be due to beam overlap during anlysis. Mes = mesostasis; SiO_2 = SiO_2 glass; n.r. = no Raman spectra obtained.

(Table 2). The cryptocrystalline ferrous silicate chondrules with FeNi-metals described by Krot et al. (2000a) differ from the SRCs described here not only in their small size but also in high FeO-contents of up to 22.9 wt%. However, one striking compositional characteristic of almost all SRCs is their depletion in the refractory elements Ca, Al, and Ti (Fig. 4 and Table 2).

Some of the non-typical SRCs have a complex mineralogy and an unusual chemical composition. The most interesting of these are 2 Mn-rich chondrules (Figs. 2g and 2h). The first (Fig. 2g) contains pyroxenes with 6.68 wt% MnO and 1.80 wt% Cr_2O_3, respectively. Pyroxenes with such high MnO concentrations have never been encountered in meteorites. Rubin (1984) reported MnO-rich orthopyroxenes in a rim around an Allende chondrule with MnO concentrations of about 4.5 wt%, and Hutchinson (1987) found a Mn-rich augite (MnO = 2.6 wt%) in the matrix of the Tieschitz chondrite. Klöck et al. (1989) reported MnO-rich olivines and pyroxenes with up to 5 wt% MnO in interplanetary dust particles. The high Mn and Cr contents of the 2 objects are clearly visible in Fig. 4, where SRC compositions are plotted relative to CI and normalized to Si = 10^6 atoms. A compositional profile (marked in Fig. 2g) over 1 pyroxene lath and the adjacent mesostasis is shown in Fig. 5. The mesostasis between the 2 pyroxene crystals has high concentrations of SiO_2, Al_2O_3, Na_2O, and K_2O, which are decreasing toward the pyroxene. In contrast, the concentrations of FeO, MnO, MgO, Cr_2O_3, and CaO are low in the mesostasis and increase toward the pyroxene. The pyroxene has a complex zoning pattern: Some elements such as Mg, Cr, and Ca show strong zoning within the pyroxene crystal, while other elements are uniformly distributed (Si, Ti, etc.). The mesostasis consisting mainly of plagioclase and some kalifeldspar contains the unidentified SiO_2 polymorph mentioned above (Table 2). The bulk composition of this exotic chondrule is high in moderately volatile elements like Mn, Cr, Na, and K, and it also has relatively high Ca and Al concentrations, as can be seen in Fig. 4.

The second Mn-rich SRC chondrule (Fig. 2h) contains pyroxenes with very high MnO and especially Cr_2O_3 concentrations of up to 3.10 and 2.49 wt%, respectively (Fig. 4). However, the accuracy of the analysis of the pyroxenes is limited because of the small size of the pyroxene crystals.

Micro-Raman and TEM Analyses of SRCs

Micro-Raman studies revealed that silica occurs in 4 different polymorphs: glass, α-quartz, cristobalite, and a thus far not identified polymorph (Figs. 2 and 6; Table 1). In addition, the silicate phase may be either glassy or crystalline. Apparently, no correlation exists between silica polymorph and the type of SRC. For example, if blebs of one phase occur within the other, the silica is either α-quartz, cristobalite, or glass (Figs. 2a, 2c, 2e, and 2f). Also, of the 2 MnO-rich silica containing chondrules, 1 contains cristobalite and the other contains the unidentified polymorph (Figs. 2g and 2h). However, the absence of systematic trends within the various types of SRCs may simply reflect insufficient statistics. At least one exception is that in all cases where the silica portion is glass, the silicate portion is also glass. Also, in all cases, crystalline silica occurs together with crystalline silicate.

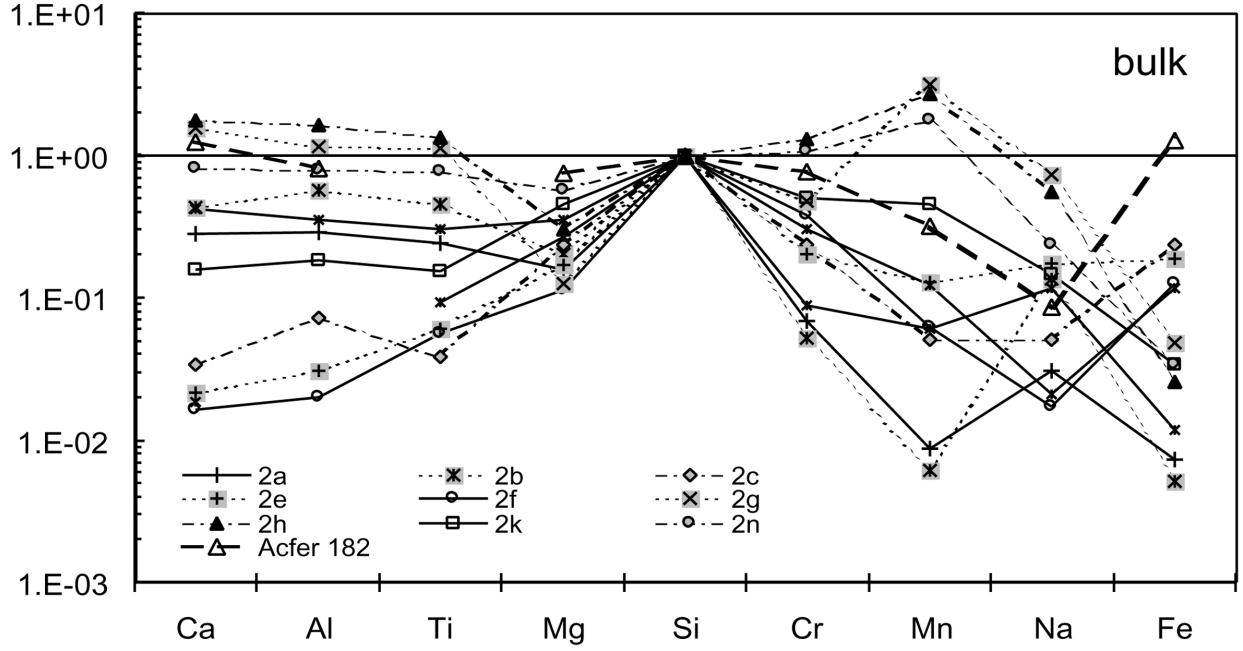

Fig. 4. Chemical composition of SRCs relative to CI and normalized to 10^6 Si. Most SRCs are depleted in refractory and in volatile elements. The bold, dashed lines indicates the bulk compositions of the 3 paired CH chondrites Acfer 182, 207, and 214 (Bischoff et al. 1993). The numbers and letters refer to the corresponding SRCs in Fig. 2.

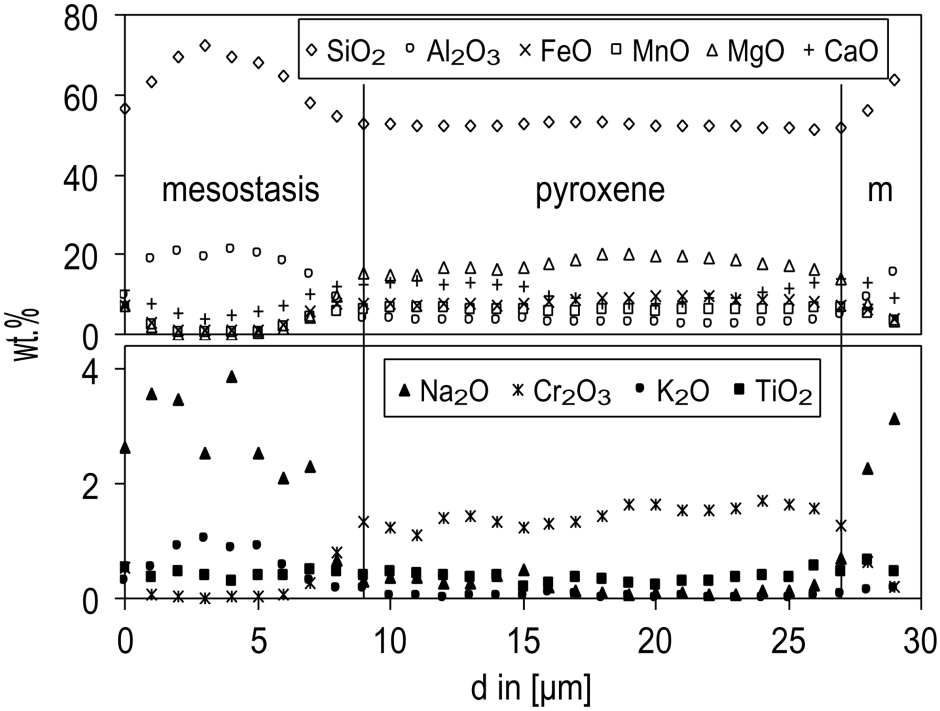

Fig. 5. Profile over 1 MnO-rich pyroxene in the SRC from Fig. 2g (see "p"). To the left and to the right, some mesostasis (m) was analyzed. See the text for detailed descriptions.

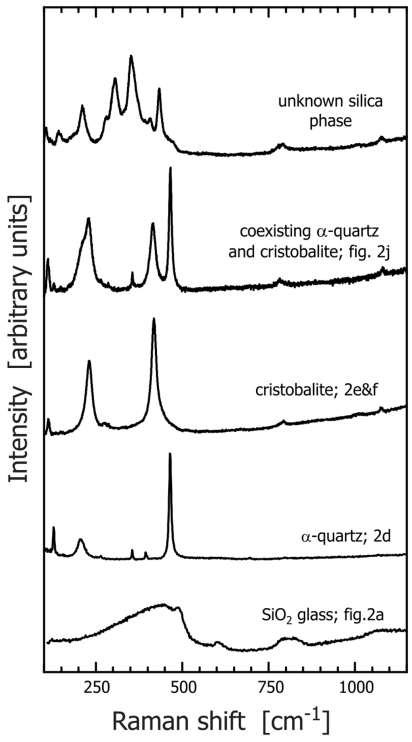

Fig. 6. Examples of micro-Raman spectra from different silica polymorphs and glass in SRCs. For band assignment, compare Bates (1972; cristobalite), Etchepare et al. (1974; α-quartz), and Sharma et al. (1981; SiO_2 glass). For tridymite reference spectra see, for instance, Etchepare et al. (1978) and Kingma and Hemley (1994), and for moganite reference spectra, see Kingma and Hemley (1994), Götze et al. (1998), and Nasdala et al. (2001).

The unidentified silica polymorph was found in a single non-typical SRC chondrule (Fig. 2g). Attempts to determine this phase by micro-Raman spectroscopy were so far unsuccessful despite comparison with spectra from quartz, tridymite, cristobalite, coesite, stishovite, moganite, and melanophlogite. We also analyzed the unknown phase using TEM and obtained a set of d-values, given in Table 3. Comparison of these d-values with a large set of d-values from known SiO_2 polymorphs did not produce a match. Further studies are in progress.

Feldspar Fragments and a Feldspar and Silica-Rich Chondrule

Large fragments of feldspar and feldspar/silica mixtures of more than 200 µm in length occur in the CH chondrite matrix (Fig. 7). The fragment in Fig. 7a is pure feldspar with anorthite contents from An_{24} to An_{27}. The cryptocrystalline fragment in Fig. 7b seems to be a 3 component mixture of approximately 80% feldspar, 20% silica, and a minor third phase that accounts for the MgO, probably pyroxene (Table 4). The single large chondrule in Fig. 8 has a complex structure: it consists of fine grained plagioclases, intergrown with quartz, including "normal" chondrule fragments. The large inclusion at the lower left in Fig. 8 is obviously of type IAB with some enclosed metal, while the 3 smaller inclusions are pyroxene crystals. The plagioclase is albite-poor, but the chondrule itself has a very Na-rich rim that can be seen in the CL image as a bright shining ring around the chondrule (Fig. 8b).

Table 3. Comparison of the d-values of the unidentified SiO_2 polymorph with some d-values from known polymorphs.[a]

u.p.	α-qtz		β-qtz		α-trd		β-trd		α-crs		β-crs		Keatite		Zeolite	
d	hkl	d	hkl	d	hkl	d	hkl	d	hkl	d	hkl	d	hkl	d	hkl	d
8.028	0 0 1	5.404	0 0 1	5.470	0 1 0	8.740	0 0 1	8.220	0 0 1	6.920	1 0 0	7.130	0 0 1*	8.604	1 0 0*	20.060
7.454	–1 1 0	4.255	–1 1 0	4.339	0 0 1	8.240	–1 1 0	4.356	1 0 0	4.970	1 1 0	5.042	1 0 0*	7.456	0 1 0*	19.800
7.391	1 0 0	4.255	1 0 0	4.339	0 1 1	5.996	1 0 0	4.356	0 1 1	4.037	1 1 1	4.117	0 1 1	5.635	1 1 0	14.092
4.970	–1 1 1	3.343	–1 1 1	3.399	1 0 0	5.040	0 0 2	4.110	1 1 0	3.514	2 0 0	3.565	1 1 0	5.272	0 0 1*	13.360
4.618	0 1 1	3.343	0 1 1	3.399	0 2 0	4.370	–1 1 1	3.849	0 0 2	3.460	2 1 0	3.189	1 1 1	4.495	1 0 1*	11.120
4.348	0 0 2	2.702	0 0 2	2.735	1 1 0	4.366	0 1 1	3.849	1 1 1	3.133	2 1 1	2.911	0 0 2*	4.302	0 1 1*	11.075
4.277	–2 1 0	2.457	–2 1 0	2.505	1 0 1	4.300	–1 1 2	2.989	1 0 2	2.840	2 2 0	2.521	2 0 0	3.728	2 0 0	10.030
4.208	1 1 0	2.456	1 1 0	2.505	0 0 2	4.120	1 0 2	2.989	2 0 0	2.485	2 2 1	2.377	1 0 2	3.726	0 2 0	9.900
3.727	–1 1 2	2.281	1 0 2	2.314	0 2 1	3.861	0 0 3	2.740	1 1 2	2.466	3 0 0	2.377	0 2 1	3.421	1 1 1	9.695
3.599	1 0 2	2.281	–1 1 2	2.314	1 1 1	3.858	–2 1 0	2.515	0 2 1	2.339	3 1 0	2.255	2 1 0	3.334	2 1 0	8.947

[a]"u.p. in the first column means "unknown polymorph;" "d" is the d-value of the interplanar spacing and "hkl" is the corresponding hkl-value. We compared the d-values of the unknown polymorph with more than those shown in the table. The table represents just a sample of the most common polymorphs.

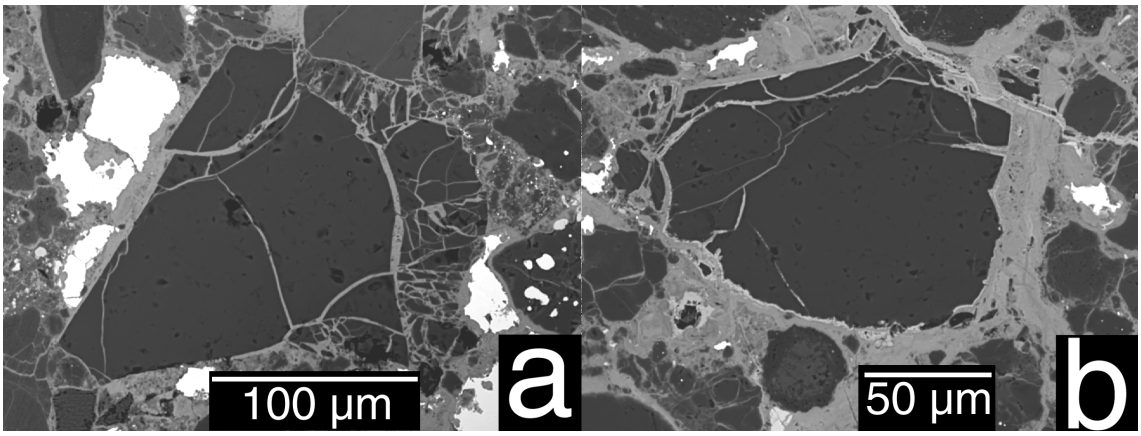

Fig. 7. BSE-images of two large, individual feldspar grains in the matrix.

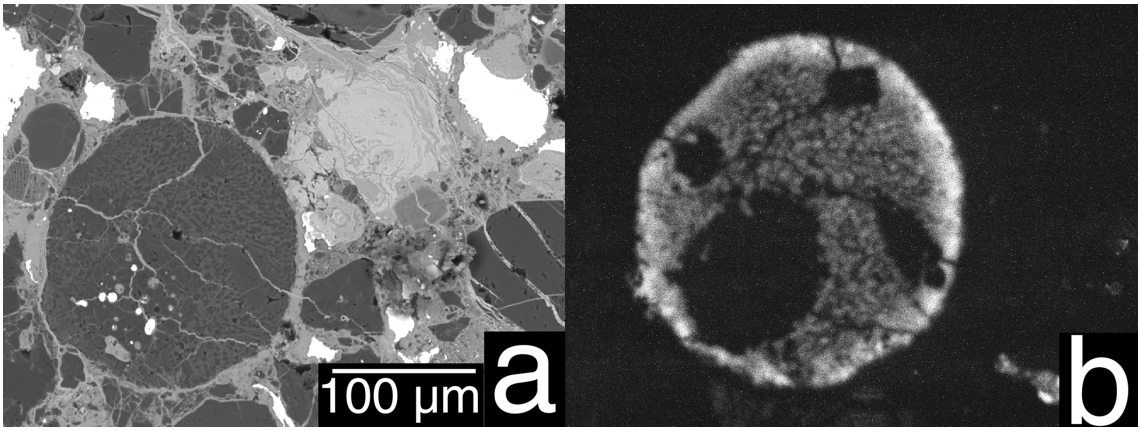

Fig. 8. BSE image (a) of a feldspar and quartz-rich chondrule with 4 inclusions, which can be seen as dark spots in the CL-image (b). The big inclusion on the left is of type IAB. The other 3 are pyroxenes. The bright rim in (b) corresponds to high Na-concentrations.

DISCUSSION

A Model for the Formation of SRCs

The high SiO_2 contents of the SRCs require an effective process for SiO_2-enrichment. Three different possibilities exist: 1) reduction of pyroxene according to the equation:

$$2MgFe[Si_2O_6] \rightarrow Mg_2[Si_2O_6] + 2Fe + 2SiO_2 + O_2$$

2) magmatic differentiation of chondrule melts, which enriches mesostasis in SiO_2; and 3) fractional condensation. The first 2 possibilities can be excluded because: 1) the reduction of enstatite produces a significant amount of metal, which is not observed in the SRCs; and 2) the SRCs cannot

Table 4. Chemical compositions of the feldspar fragments.

Mineral number	Fig. 9a Fsp	Fig. 9b Fsp
SiO_2	60.79	72.88
TiO_2	0.03	0.06
Al_2O_3	23.81	16.28
Cr_2O_3	0.01	0.02
FeO	1.12	0.47
MnO	0.01	0.03
NiO	0.07	0.04
MgO	0.10	2.34
CaO	5.61	1.73
Na_2O	8.51	6.86
K_2O	0.13	–
Total	100.19	100.70

have previously been mesostasis because they are depleted in refractory elements (Ca, Al, and Ti), while normal chondrule mesostasis is enriched in these elements. Therefore, we favor fractional condensation (3) as the process for SiO_2-enrichment. The preference for fractional condensation is also based on the study of the layered object in Fig. 3, which provides strong evidence for fractional condensation, as will be shown in the following section.

The possibility of silica condensation was indicated by Petaev and Wood (1998) in their "condensation with partial isolation" (CWPI) model and proposed by Krot et al. (2000b) for the formation of silica-rich rims around CR chondrites and by Hezel et al. (2002b) for SRCs in CH chondrites. In the CWPI-model, a certain fraction of condensed minerals behaves chemically inert against the remaining nebular gas. A nebula of solar composition will first condense CAI-like material and, subsequently, the main components forsterite, FeNi-metal, enstatite, and plagioclase (e.g., Petaev and Wood 1998; Ebel and Grossman 2000). As the nebula has an initial atomic Mg/Si ratio of ~1, it will become substantially enriched in SiO, the major Si-bearing gas species, during forsterite condensation because forsterite incorporates twice the number of Mg atoms as Si. Enstatite is the next silicate phase to condense. If condensation of enstatite occurs by reaction of gaseous SiO with condensed forsterite, the amount of Si atoms in the nebula will decrease due to the reaction:

$$Mg_2SiO_4\,(s) + SiO\,(g) + \tfrac{1}{2}O_2\,(g) = 2MgSiO_3\,(s)$$

If, however, enstatite condenses separately without reacting with the olivine according to:

$$Mg(g) + SiO\,(g) + \tfrac{1}{2}O_2\,(g) = MgSiO_3\,(s)$$

the same number of Si and Mg atoms will be removed from gas, leading to a relative increase of the Si/Mg ratio in the remaining gas and, thus, allowing condensation of SiO_2 at lower temperatures. Thus, condensation of SiO_2 requires the removal of forsterite from reactive contact with the nebula, i.e., fractional condensation.

Petaev and Wood (1998) call the fraction of inert phases the "isolation degree (ξ)." They calculated that for $\xi > 0.47$, silica would appear as a condensate at around 1230 K. The unique object shown in Fig. 3 documents the fractional condensation process and the late appearance of silica. We assume that the central region of this chondrule formed from an early condensed melt that was rich in Mg, Ca, and Al (e.g., Ebel and Grossman 2000). During subsequent cooling, olivine crystallized from the chondrule melt and remained inert against the nebula, which, thereby, was enriched in silica. In the next step, metal and, shortly thereafter, pyroxene condensed. Some nebular Si reacted with the peripheral olivine of the object, thereby forming the rim pyroxene. This reaction is recorded in the olivines that are completely or partially enclosed in the pyroxenes. However, some pyroxene must have condensed independent of olivine to produce the high-Si gas that ultimately leads to the silica condensates at the rim. Similar zoned type IA chondrules were described previously in CR chondrites (Noguchi 1995; Krot et al. 2000b, 2002, 2003). Brigham et al. (1986) also proposed some kind of fractional condensation process for the formation of silica-rich objects in ordinary chondrites.

In some cases, SiO_2 phases may separately condense without being attached to previously condensed pyroxenes. SRC precursors will then form by agglomeration of such phases, occasionally including some pyroxene and/or olivine.

After the formation of SRC precursors, these were reheated to at least 1968 K. This temperature is based on 2 lines of evidence: 1) the SRC texture and 2) the silica polymorphs of the SRCs. 1) Several SRCs contain blebs of silica in a silicate matrix or vice versa (Figs. 2a, 2c, 2e, 2f, 2m, and 2n). This texture can be explained by the formation of SRCs within the liquid immiscibility gap in the system MgO-SiO_2-FeO (Fig. 9). Above a temperature of 1968 K, a silicate melt and a nearly pure SiO_2 melt coexist and, as a consequence, 1 of the 2 melt phases will line out, minimize its surface tension, and form blebs within the other melt phase (Figs. 9 and 10). These SiO_2 blebs can be seen in Figs. 2a, 2c, 2e, 2f, 2m, and 2n. However, not all SRCs form these blebs. In some occurrences (Figs. 2b, 2i, and 2o), silica and silicate still have rounded interfaces but appear in a cockscomb or symplectitic texture. The various textures may depend on cooling rate and/or the excess temperature above the liquidus temperature. 2) The second evidence for the reheating event comes from micro-Raman spectroscopy. Silica in various SRCs appears in several polymorphs: glass, α-quartz, and cristobalite (Fig. 6). The formation of cristobalite as the high temperature polymorph of silica requires at least 1743 K (Heaney 1994). In addition, glass, which is quenched melt, must have formed initially above 1968 K. The occurrence of different silica polymorphs and either glassy or crystalline silicate in different SRCs are probably indicative of variable cooling rates: very fast cooling to form the glassy objects and slower cooling to form

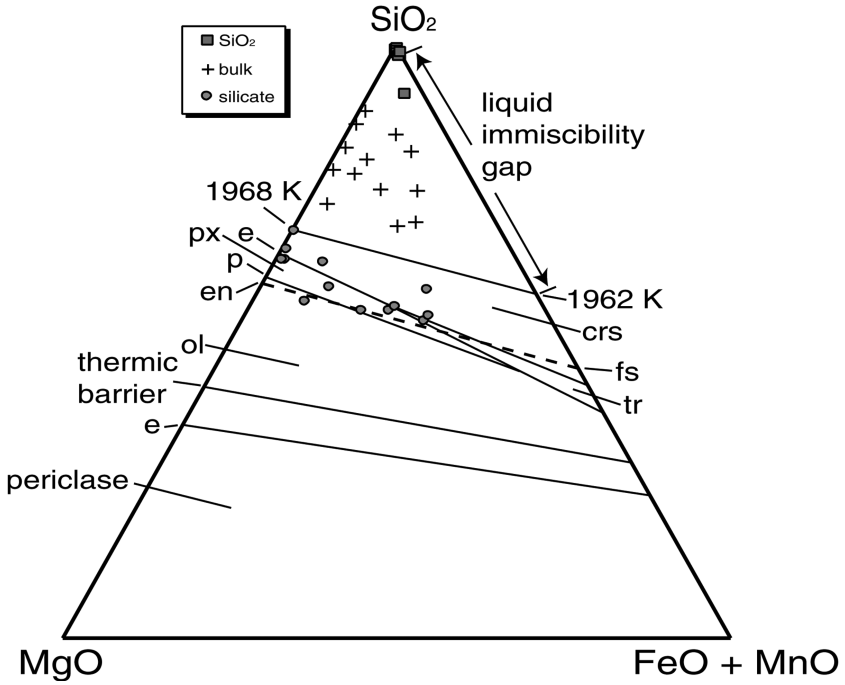

Fig. 9. Ternary phase diagram of the system MgO-SiO_2-FeO after Bowen and Schairer (1935). "SiO_2" is the analyzed silica, and "silicate" is the analyzed silicate portion of the SRCs. "Bulk" is the calculated bulk composition of the SRCs; e = eutectic point; p = peritectic point.

the crystalline ones. Also, the glassy SRCs, possibly, were heated to higher temperatures at which most or all crystallization nuclei were destroyed. Then, crystallization could have been much slower and they may have experienced the same cooling rate as the SRCs with crystalline silica and silicate. Silicates are sometimes silica oversaturated with respect to pyroxene composition (Fig. 9). This happened when the silicate melt did not reach the eutectic point during cooling and solidified at elevated temperatures, above 1816 K (Figs. 9 and 10).

From these 2 lines of evidence (the SRC texture and the high temperature silica polymorphs), we conclude that the SRCs were reprocessed at high temperatures. The peak temperature was at least 1968 K, which is the minimum temperature for the liquid immiscibility in the MgO-SiO_2 system. Even FeO-rich compositions would not decrease the minimum temperature significantly, as the liquidus temperature in the FeO-SiO_2 system is 1962 K (Fig. 9). The occurrence of cristobalite as well as silica and silicate glass require high temperatures for the reheating event, and the occurrence of glass obviously also demands minimum temperatures of 1968 K. Cooling must have been very fast after reheating, otherwise high-temperature polymorphs like cristobalite and glass could not have been preserved.

From these interpretations, we conclude a 2-stage model for the formation of the SRCs (Fig. 11). In the first stage, the SRC precursors formed late during fractional condensation and, subsequently, these precursors were reheated to at least 1968 K and then cooled very quickly. The significant variations of FeO-concentrations in SRCs (Table 2; Fig. 9) may result from oxidizing conditions during reheating, leading to a redistribution and oxidation of Fe from FeNi metal to silicates, as experimentally demonstrated by Dohmen et al. (1998).

Cooling and Formation of Some Particular SRCs

In some SRCs, a particular record of heating and cooling is preserved. The SRCs in Figs. 1a and 2a are divided into a core and a mantle region. This texture may have developed within the liquid immiscibility gap. Figure 12 illustrates a possible mechanism: the SRC precursor was heated to a peak temperature well above the opening of the immiscibility gap. During cooling or at T_{max}, the liquid SRC decomposed into silica liquid (L_2), which formed the mantle, and silicate liquid (L_1), which formed the core region. After further cooling, the core decomposed again into liquid silica blebs (L_4) and liquid silicate mesostasis (L_3). Further rapid cooling led to the present texture with glassy silica and silicate.

In Fig. 2c, the spherules are silica and the matrix is hypersthene normative. TEM analyses revealed that silica is present as tiny, nanocrystalline α-quartz grains, which are often twinned according to the brazil law (Fig. 13). The now nanocrystalline silica spherules were, most probably, initially glass that was metastable and subsequently devitrified to cristobalite-tridymite and then to α-quartz. As Acfer 182 is classified as shock-stage 2, the twinning is most probably the result of shock, as brazil twins form as a response to stress (P. Heaney, personal communication). In this case, artificial structural changes induced during ion-milling can be

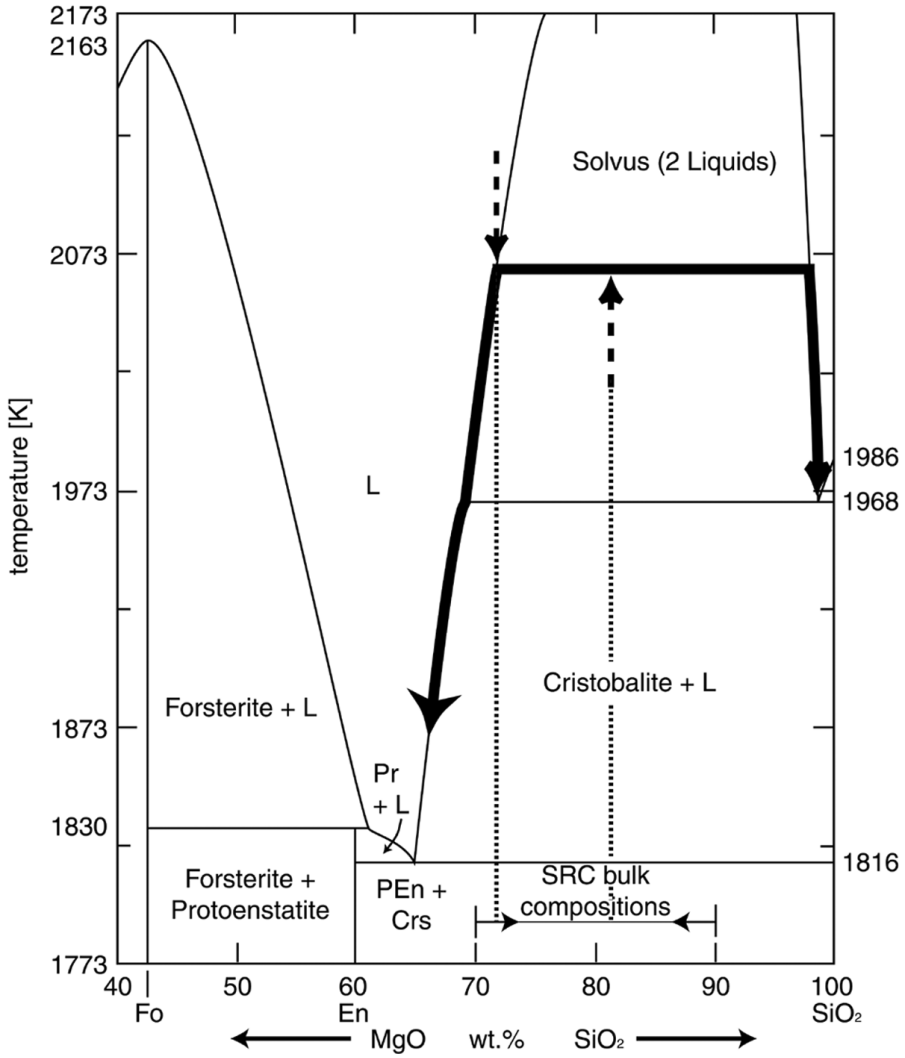

Fig. 10. Part of the binary phase diagram of the MgO-SiO_2 system (Morse 1980, and references therein). The bold line shows a possible cooling path after the reheating event. The formation of the SRC texture with blebs of silica or silicate within silicate or silica, respectively, occurred in the liquid immiscibility gap above 1968 K. After reheating, both liquids cooled and cristobalite or silica glass formed at 1968 K. The silicate liquid cooled further and reached the eutectic point at 1816 K or converted to glass before the eutectic point. If it reached the eutectic point, pyroxene was able to crystallize.

excluded, as brazil twins would not be produced during this procedure.

The SRC-like chondrule in Fig. 2g is extremely enriched in MnO (up to 6.86 wt%; Table 2; Fig. 4; Fig. 5). This is unusual as the bulk meteorite has only 0.13 wt% MnO and as the average MnO contents of chondrules in CH chondrites is usually below 0.5 wt% (Bischoff et al. 1993). However, this object has comparatively high CaO and Al_2O_3 contents. The high concentration of MnO in the pyroxenes is the result of the high bulk silica content of the chondrule. In a high silica rhyolitic melt (compositionally similar to this SRC), the partition coefficient of MnO between pyroxene and melt is very high. The K_D-values for high- and low-Ca pyroxenes are approximately the same, between 30 and 34 for high- and between 25.4 and 71.3 for low-Ca pyroxene (e.g., Mahood and Hildreth 1983; Ewart and Griffin 1994). The calculated MnO concentrations in this SRC are between 5.51 (K_D = 30) and 6.24 wt% (K_D = 34). These theoretical values are in good agreement with the measured mean concentrations of 6.37 wt% MnO. The profile over one pyroxene in this SRC (Fig. 5) shows a normal zoning pattern, as expected for a pyroxene that crystallized from a melt and, thus, supports the idea of Mn-incorporation into the pyroxene during crystallization in a rhyolite-normative melt. A second Mn-rich chondrule (Table 2; Fig. 2h) has tiny pyroxene crystals with an even narrower mesostasis around them. This circumstance, unfortunately, causes some beam overlap during electron microprobe analysis so that no accurate partition coefficient for Mn can be determined. The high MnO-concentrations also result in a very high MnO/FeO ratio of ~1 for bulk composition

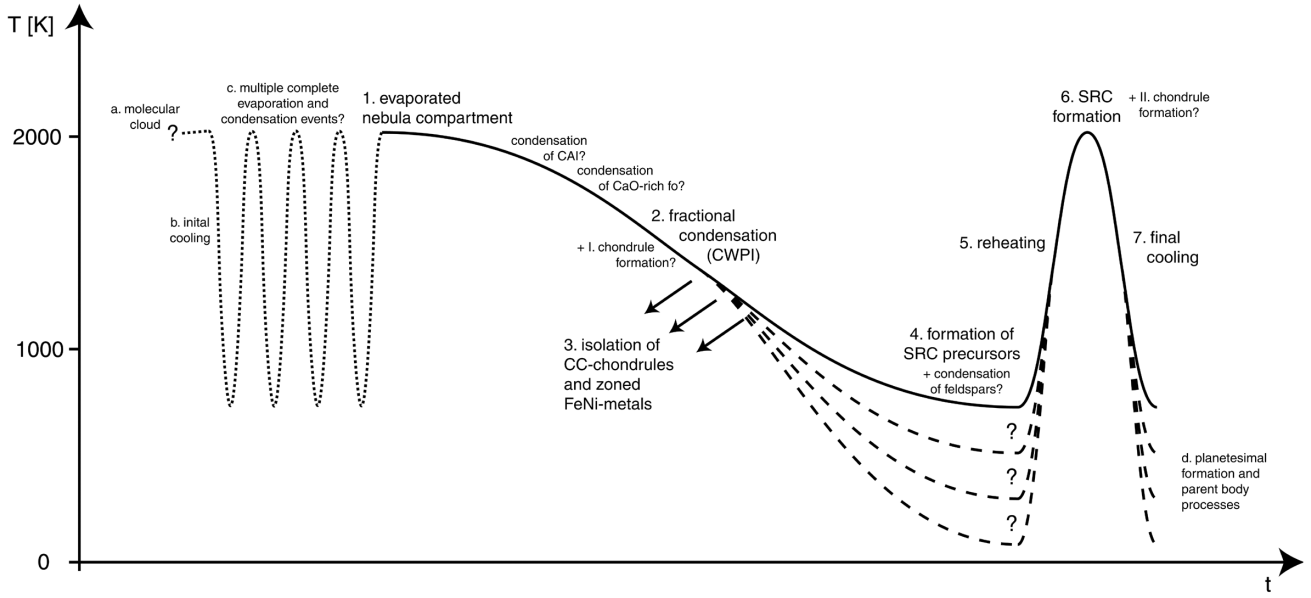

Fig. 11. A possible chronology for the formation of CH chondrite components. Two episodes are indicated: first, a fractional condensation of SiO_2-rich precursors and possibly metals, and second, a reheating of at least SiO_2-rich material. See the text for detailed descriptions.

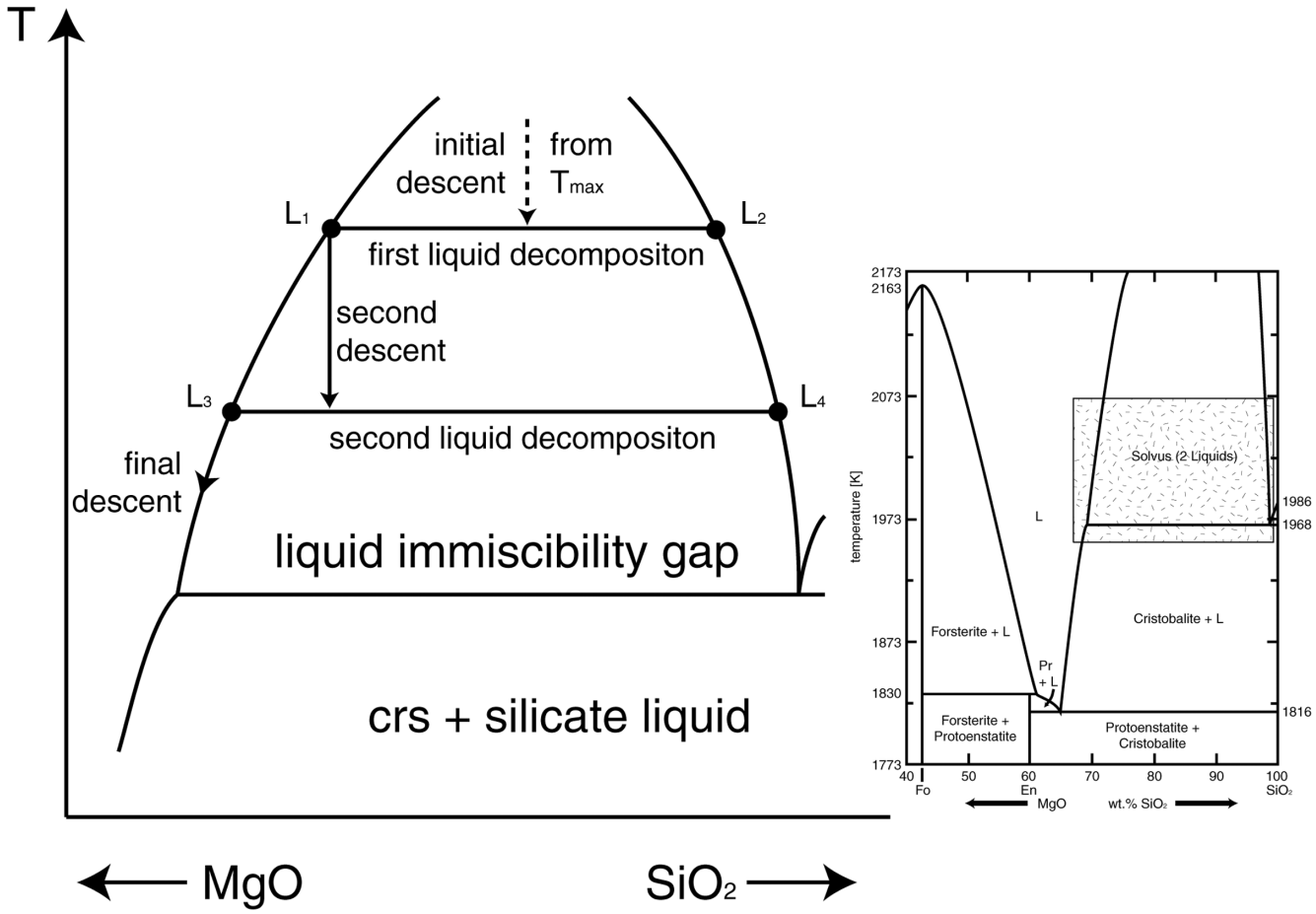

Fig. 12. Part of the phase diagram shown in Fig. 10 illustrating the formation of the SRC shown in Figs. 1a and 2a, respectively.

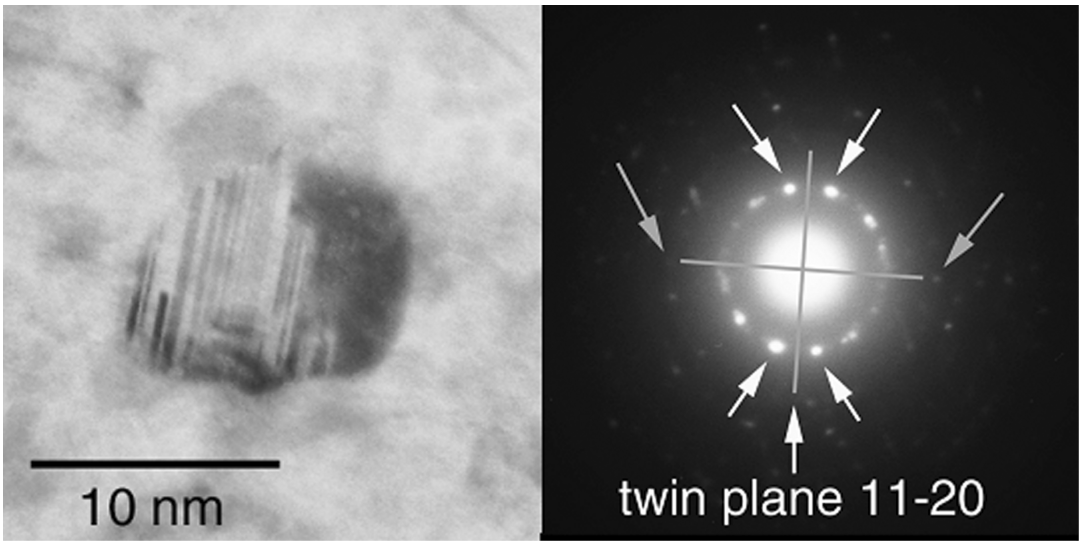

Fig. 13. Bright-field (a) and diffraction (b) TEM images of a nanocrystalline quartz grain in one of the silica blebs in the SRC fragment of Fig. 2c. The alternating black and white lines in the bright-field image are twins after the brazil law, as can be seen from the diffraction pattern in (b).

as well as for the pyroxenes in these 2 SRCs. Petaev et al. (2001) also found high enrichments of MnO in pyroxenes within silica-bearing objects.

Manganese enrichment in the nebular gas may have occurred during fractional condensation at similar temperatures as Si-enrichment. At temperatures where most of the Mg is condensed as olivine and pyroxene and some uncondensed Si is left in the gas, Mn will be mainly present as Mn gas. Since a large fraction of Si is condensed, the Mn/Si ratio in the gas will be rather high. If further nebular cooling is fast, Si and Mn will both condense together leading to Si- and Mn-rich assemblages.

The "MELTS" code of Ghiorso and Sack (1995) give liquidus temperatures of 1674 K for the Mn-rich chondrule 1 and 1900 K for the Mn-rich chondrule 2, indicating high temperatures during the reheating process. Therefore, this Mn-rich object supports the idea of fractional condensation in the first stage and a reheating event in the second stage of SRC formation.

The silica-rich objects with large olivine crystals surrounded by orthopyroxene and a silica-rich mesostasis with silica laths (Fig. 2l) may have resulted from precursors with pyroxene and silica and relatively large quantities of olivine. During the reheating event, these objects did not melt completely like other SRCs due to the high olivine content. Mesostasis may have melted and reacted with the olivines, thereby forming the orthopyroxene.

The Formation of Metal Within the 2-Stage Formation Process

Meibom et al. (1999, 2000) found that Ni, Co, and Cr are zoned in some FeNi metal grains of the CH chondrites. These authors correlated the patterns of these elements with thermodynamically calculated zoning patterns and concluded that they correspond to fast gas-solid condensation (~0.4 K/h) of the FeNi metal grains from nebular gas. This conclusion was recently confirmed by additional trace element analyses (Cu, Ru, and Pd) in the zoned FeNi metal grains by Campbell and Humayun (2002). The preservation of these zoning patterns requires temperatures below ~800 K. Therefore, these metals must have remained in a relatively cold environment after formation. So far, these metals were taken as evidence that these meteorites experienced only 1 cooling event and, hence, are among the most primitive meteorites we know.

The existence of these zoning patterns is in obvious contradiction to the postulated reheating event in the second stage of SRC formation and the formation of Mn-rich objects. As a consequence, the primitive status of the CH chondrites must be partially revised. On one hand, primitive components undoubtedly exist in these meteorites (zoned metals), but on the other hand, the meteorites also contain reprocessed components (SRCs). Therefore, at least the zoned metals must have been isolated within or from the nebula compartment before the reheating process took place. Maybe these metals were simply removed from the nebula compartment, although this removal process itself remains enigmatic.

Formation of Feldspars

The feldspar and feldspar/quartz fragments (Fig. 7) may represent another late product in the fractional condensation sequence, besides SRC precursors. In the CWPI calculations of Petaev and Wood (1998), plagioclase appears shortly before silica (1215 K) in the interval between 1275 K (anorthite) and 1218 K (albite) at P_{tot} = 10 Pa and an isolation degree of around

$\xi \approx 1\%$. Plagioclase condensation would remove Na from the gas. The condensation of feldspar shortly before silica could explain why most SRCs are so low in volatile elements such as Na. Another possibility is that the SRCs lost their moderately volatile and volatile elements during the reheating event. Further investigation of Mg and Si isotopes are necessary to determine whether or not evaporation occurred.

Formation of "Normal" Chondrules

As the second stage of SRC formation requires high temperatures, the chondrule forming event could have happened together with the reheating event. On the other hand, evidence exists for an earlier chondrule formation event. The plagioclase-rich object shown in Fig. 8 has inclusions compositionally similar to normal chondrule fragments. The boundary of the inclusions with the chondrule matrix has no obvious reaction texture and, therefore, implies that the inclusion was cold and the chondrule melt close to complete crystallization at the time of collision and incorporation of the inclusion into the plagioclase-rich object. Therefore, this texture postdates the solidification of the plagioclase-rich object after the formation of normal chondrules. Therefore, during the initial cooling and fractional condensation, transient and discrete heating events could have occurred, leading to normal chondrule formation. In combination, 2 normal chondrule forming events are conceivable: a limited and less effective process during initial cooling and a second process during reheating (Fig. 11). These localized heating events may also have influenced the metal formation. Perhaps some of the now unzoned metals lost their zoning pattern during 1 of these localized heating events.

Formation of Cryptocrystalline Chondrules

Krot et al. (2001) described a possible mechanism for the formation of cryptocrystalline (CC) and skeletal olivine (SO) chondrules in the CB chondrites. In this model, the chondrule melts condensed directly from a completely evaporated, hot nebula region. As CC and SO chondrules lack volatile elements, they must have been removed from the formation location at elevated temperatures and then cooled rapidly. As the CH chondrites are related to the CB chondrites as outlined in the introduction, their cryptocrystalline chondrules may have formed in the same way as those in the CB chondrites. The CC and SO chondrules may have formed during fractional condensation and were already removed from the nebula compartment during this first cooling (Fig. 11).

SUMMARY

We propose a 2-stage model for the formation of the CH chondrite components (the following numbers and letters correspond to Fig. 11): (1) The formation model for the CH chondrites begins with a completely evaporated nebula compartment, as indicated by the solid line in Fig. 11. (2) During cooling, fractional condensation occurred. (3) The first condensates were CAIs followed by olivine, metal, pyroxene, feldspar, and silica. Cooling was interrupted by transient and discrete heating events that lead to the formation of "normal" chondrules (type I and II porphyritic chondrules, barred chondrules, etc.). Some metals developed zoning patterns, reflecting fractional condensation. Cryptocrystalline chondrules and metals were, at least partially, removed or isolated from the nebula compartment. (4) Fractional condensation produced silica-rich material at low temperatures that served as a precursor for the SRCs. The ambient temperature of the solar nebula is unknown, as indicated by the dashed lines in Fig. 11. (5) During reheating, these precursors experienced temperatures above 1968 K. This event may also have produced chondrules. (6) The SRC precursors reached the liquid immiscibility gap of the system MgO-SiO_2-FeO and formed their present texture. (7) Many SRCs retain high temperature polymorphs of silica or silica glass, implying fast cooling. In addition, some melts were quenched at higher temperatures above the eutectic point. This points to rapid cooling after reheating. (d) Finally, SRCs were incorporated into planetesimals.

Acknowledgments–Dominik C. Hezel is grateful for the support of this work by the Deutschen Akademischen Auslandsdienst (DAAD). We also thank Peter Heaney for the discussion about twinning and cooling of silica. The authors thank Pedro Garcia for providing excellent thin sections and Markus Klein for microprobe maintenance. Special thanks from D. Hezel to Thorbjörn Schönbeck and Andreas Pack for fruitful discussions. The authors are grateful to A. N. Krot and an anonymous reviewer for their thorough and helpful reviews and to the MAPS associate editor K. Righter for his work and helpful comments.

Editorial Handling—Dr. Kevin Righter

REFERENCES

Bates J. B. 1972. Raman spectra of α and β cristobalite. *Journal of Chemical Physics* 57:4042–4047.

Bischoff A., Palme H., Schultz L., Weber D., Weber H. W., and Spettel B. 1993. Acfer 182 and paired samples, an iron-rich carbonaceous chondrite: Similarities with ALH 85085 and relationship to CR chondrites. *Geochimica et Cosmochimica Acta* 57:2631–2648.

Bowen N. L. and Schairer J. F. 1935. The system MgO–FeO–SiO_2. *American Journal of Science* 29:151–217.

Brearley A. J. and Jones R. H. 1998. Chondritic meteorites. In *Reviews in mineralogy: Planetary materials,* edited by Papike J. J. Washington, D. C.: Mineralogical Society of America. 398 p.

Brigham C. A., Yabuki H., Ouyang Z., Murrell M. T., El Goresy A., and Burnett D. S. 1986. Silica-bearing chondrules and clasts in ordinary chondrites. *Geochimica et Cosmochimica Acta* 50: 1655–1666.

Campbell A. J. and Humayun M. 2002. Condensation of metal in a CH chondrite. *Meteoritics & Planetary Science* 37:A29.

Dohmen R., Chakraborty S., Rammensee W., and Palme H. 1998. Solid-solid reactions mediated by a gas phase: An experimental study of reaction progress and the role of surfaces in the system olivine + Fe-metal. *American Mineralogist* 83:970–984.

Ebel D. S. and Grossman L. 2000. Condensation in dust-enriched systems. *Geochimica et Cosmochimica Acta* 64:339–366.

Etchepare J., Merian M., and Smetankine L. 1974. Vibrational normal modes of SiO_2. I. α and β quartz. *Journal of Chemical Physics* 60:1873–1876.

Etchepare J., Merian M., and Kaplan P. 1978. Vibrational normal modes of SiO_2. II. Cristobalite and tridymite. *Journal of Chemical Physics* 68:1531–1537.

Ewart A. and Griffin W. L. 1994. Application of proton-microprobe data to trace-element partitioning in volcanic rocks. *Chemical Geology* 117:251–284.

Ghiorso M. S. and Sack R. O. 1995. Chemical mass transfer in magmatic processes. IV. A revised and internally consistent thermodynamic model for the interpolation and extrapolation of liquid-solid equilibria in magmatic systems at elevated temperatures and pressures. *Contributions to Mineralogy and Petrology* 119:197–212.

Götze J., Nasdala L., Kleeberg R., and Wenzel M. 1998. Occurrence and distribution of "moganite" in agate/chalcedony: A micro-Raman, Rietfeld, and cathodoluminescence study. *Contributions to Mineralogy and Petrology* 133:96–105.

Greshake A., Krot A. N., Meibom A., Weisberg M. K., Zolensky M. E., and Keil K. 2002. Heavily-hydrated lithic clasts in CH chondrites and the related, metal-rich chondrites Queen Alexandra Range 94411 and Hammadah Al Hamra 237. *Meteoritics & Planetary Science* 37:281–293.

Grossman J. N., Rubin A. E., and MacPherson G. J. 1988. ALH 85085: A unique volatile-poor carbonaceous chondrite with possible implications for nebular fractionation processes. *Earth and Planetary Science Letters* 91:33–54.

Heaney P. J. 1994. Structure and chemistry of the low-pressure silica polymorphs. In Silica: Physical behavior, geochemistry, and materials applications, edited by Heaney P. J., Prewitt C. T., and Gibbs G.V. Washington D.C: Geological Society of America. pp. 1–40.

Hezel D. C., Brenker F. E., and Palme H. 2002a. Petrology and cooling history of cryptocrystalline chondrules from CH chondrites (abstract #1787). 33rd Lunar and Planetary Science Conference.

Hezel D. C., Brenker F. E., Palme H. 2002b. An unusual population of silica-rich components (SRC) in the CH chondrites Acfer 182 and 207. *Meteoritics & Planetary Science* 37:A63.

Hutchinson R. 1987. Chromian manganoan augite in the interchondrule matrix of the tieschitz (H3) chondritic meteorite. *Mineralogical Magazine* 51:311–316.

Ivanova M. A., Petaev M. I., Clayton R. N., Mayeda T. K., Hutcheon I. D., Phinney D., Nazarov M. A., Taylor L. A., and Wood J. A. 2001. NWA 470, A new CH chondrite from the Moroccan Sahara (abstract #1817). 33rd Lunar and Planetary Science Conference.

Kingma K. J. and Hemley R. J. 1994. Raman spectroscopic study of microcrystalline silica. *American Mineralogist* 79:269–273.

Klöck W., Thomas K. L., McKay D. S., and Palme H. 1989. Unusual olivine and pyroxene composition in interplanetary dust and unequilibrated ordinary chondrites. *Nature* 339:126–128.

Koblitz J. 2000. Metbase 5.0.

Kretz R. 1983. Symbols for rock-forming minerals. *American Mineralogist* 68:277–279.

Krot A. N., Meibom A., Petaev M. I., Keil K., Zolensky M. E., Saito A., Mukai M., and Ohsumi K. 2000a. Ferrous silicate spherules with euhedral iron-nickel metal grains from CH carbonaceous chondrites: Evidence for supercooling and condensation under oxidizing conditions. *Meteoritics* 35:1249–1258.

Krot A. N., Weisberg M. K., Petaev M. I., Keil K., and Scott E. R. D. 2000b. High-temperature condensation signatures in type I chondrules from CR carbonaceous chondrites. (abstract #1470). 31st Lunar and Planetary Science Conference.

Krot A. N., Meibom A., Russell S. S., Alexander C. M., Jeffries T. E., and Keil K. 2001. A new astrophysical setting for chondrule formation. *Science* 291:1776–1779.

Krot A. N., Meibom A., Weisberg M. K., and Keil K. 2002. The CR chondrite clan: Implications for early solar system processes. *Meteoritics & Planetary Science* 37:1451–1490.

Mahood G. and Hildreth W. 1983. Large partition coefficients for trace elements in high silica rhyolites. *Geochimica et Cosmochimica Acta* 47:11–30.

Meibom A., Petaev M. I., Krot A. N., Wood J. A., and Keil K. 1999. Primitive FeNi metal grains in CH carbonaceous chondrites formed by condensation from a gas of solar composition. *Journal of Geophysical Research* 104:22053–22059.

Meibom A., Desch S. J., Krot A. N., Cuzzi J. N., Petaev M. I., Wilson L., and Keil K. 2000. Large scale thermal events in the solar nebula: Evidence from FeNi metal grains in primitive meteorites. *Science* 288:839–841.

Morse S. A. 1980. *Basalts and phase diagrams.* New York: Springer-Verlag. 493 p.

Nasdala L., Banerjee A., Häger T., and Hofmeister W. 2001. Laser-raman micro-spectroscopy in mineralogical research. *Microscopy and Analysis* 70:7–9.

Noguchi T. 1995. Petrology and mineralogy of the PCA 91082 chondrite and its comparison with the Yamato-793495 (CR) chondrite. *Proceedings of the NIPR Symposium on Antarctic Meteorites* 8:33–62.

Petaev M. I. and Wood J. A. 1998. The condensation with partial isolation (CWPI) model of condensation in the solar nebula. *Meteoritics & Planetary Science* 33:1123–1137.

Petaev M. I. and Krot A. N. 1999. Condensation of CH chondrite materials: Inferences from the CWPI model (abstract #1775). 30th Lunar and Planetary Science Conference.

Petaev M. I., Ivanova M. A., Nazarov M. A., and Wood J. A. 2001. Silica-bearing objects in the CH-chondrite NWA 470: Evidence for their formation in fractionated nebular systems (abstract #1450). 32nd Lunar and Planetary Science Conference.

Rubin A. E. 1984. Manganiferous orthopyroxene and olivine in the allende meteorite. *American Mineralogist* 69:880–888.

Scott E. R. D. 1988. A new kind of primitive chondrite, Allan Hills 85085. *Earth and Planetary Science Letters* 91:1–18.

Sharma S. K., Mammone J. F., and Nicol M. F. 1981. Raman investigation of ring configurations in vitreous silica. *Nature* 292: 140–141.

Wasson J. T. 1988. A non-nebular origin for the Allan Hills 85085 subchondritic meteorite (abstract #1240). 29th Lunar and Planetary Science Conference.

Wasson J. T. and Kallemeyn G. W. 1990. Allan Hills 85085: Subchondritic meteorite with mixed nebular and regolithic heritage. *Earth and Planetary Science Letters* 101:148–161.

Weisberg M. K., Prinz M., and Nehru C. E. 1988. Petrology Of ALH 85085: A chondrite with unique characteristics. *Earth and Planetary Science Letters* 91:19–32.

Weisberg M. K., Prinz M., Clayton R. N., Mayeda T. K., Grady M. M., and Pillinger C. T. 1995. The CR chondrite clan. *Proceedings of the NIPR Symposium on Antarctic Meteorites* 8:11–32.

Weisberg M. K., Prinz M., Clayton R. N., Mayeda F. K., Sugiura N., Zashu S., and Ebihara M. 2001. A new metal-rich chondrite Grouplet. *Meteoritics & Planetary Science* 36:401–418.